Biogeosciences, 3, 1–13, 2006
www.biogeosciences.net/bg/3/1/
SRef-ID: 1726-4189/bg/2006-3-1
European Geosciences Union

Biogeosciences

Diatoms and their influence on the biologically mediated uptake of atmospheric CO_2 in the Arabian Sea upwelling system

T. Rixen[1], **C. Goyet**[2], **and V. Ittekkot**[1]

[1]Center for Tropical Marine Ecology, Fahrenheitstr. 6, 28 359 Bremen, Germany
[2]Université de Perpignan, Bât. B., EA 1947 BDSI, 52 avenue Paul ALDUY, 66 860 Perpignan, France

Received: 17 December 2004 – Published in Biogeosciences Discussions: 25 January 2005
Revised: 4 May 2005 – Accepted: 6 December 2005 – Published: 9 January 2006

Abstract. Sediment trap experiments have been carried out in order to study processes controlling shifts from diatom to non-diatom dominated systems in the western Arabian Sea. One of our major problems was to link sediment trap records to surface ocean processes. Satellite-derived observations on upper ocean parameters were helpful to reduce this problem in the past and gain a new quality by combining it with results obtained during the Joint Global Ocean Flux Study (JGOFS) in the Arabian Sea. The new results imply that intense grazing can decline or impede the development of large diatom blooms in a silicon-enriched near shore upwelling system off Oman. In the open western Arabian Sea diatom blooms recover within the offshore advecting upwelled water and lead to peak organic fluxes into the deep sea but only during the later phase of the upwelling season. During onset of the upwelling season grazing favoured by eolian iron inputs causing the formation of thinner diatom shells seems to prevent the development of a large diatom bloom within the silicon-enriched offshore advecting upwelled water. An increased relevance of diatoms and diatom-grazing copepods in the planktonic community as well as oligotrophic conditions seem to raise the ratio between organic carbon formation and calcium carbonate carbon precipitation (rain ratio) in the surface water. The decomposition of organic matter in the water column reduces the rain ratio within in the sinking matter especially in the oligotrophic region dominated by cyanobacteria and reduces also the variation of the carbon to nutrient uptake ratios seen in the surface water.

1 Introduction

Marine organisms influence ocean/atmospheric CO_2 exchange by photosynthesising organic matter and by precipitating carbonate shells. The subsequent export of organic carbon and calcium carbonate into the deep sea and the resulting net effect on the atmospheric CO_2 concentration is defined as the biological pump (Volk and Hoffert, 1985). The biological pump is driven by nutrients such as phosphate and inorganic nitrogen (N = nitrate + nitrite + ammonia), which are, in addition to carbon, required to build up organic matter (Heinze et al., 1991; Maier-Reimer et al., 1996; Tyrrell, 1999; Hedges et al., 2002). The efficiency of the biological pump can be enhanced by raising the uptake ratio of carbon to nutrients (C/N/P Redfield ratio) during the production of organic matter and by a reduction of the calcium carbonate precipitation, because the latter process increases the CO_2 concentration in sea water (Redfield et al., 1963; Berger and Keir, 1984; Heinze et al., 1991). Depending on the species and on environmental conditions the C/P ratio of marine organisms varies between 40 and $>$200 (Goldman et al., 1979; Burkhardt et al., 1999; Geider and La Roche, 2002; Klausmeier et al., 2004). Nevertheless, despite such variations, a global analysis suggests a mean Redfield ratio of 117±14/16±1/1 (Anderson and Sarmiento, 1994), which is close to the constant Redfield ratio derived by a "General Circulation Model" (GCM, 122/16/1, Maier-Reimer, 1996), and to those found by a basin-wide analysis in the Arabian Sea (125:14:1, Millero et al., 1998).

Carbonate production is often parameterised by applying a fixed ratio between the organic carbon production and the precipitation of calcium carbonate carbon (rain ratio, Sarmiento et al., 2002). Data-based estimates of rain ratios are scarce and deviate between 3.3 and 12.5 (Sarmiento et al., 2002 and references therein). A new estimate even suggests a mean global rain ratio of 16 (Sarmiento et al., 2002). All these estimates fall within the range of global mean rain ratios (2.3 to 26.6), which can be obtained by dividing the global mean organic carbon export derived from satellite data (2 to 16 10^{15} g C yr^{-1}; Falkowski et al., 2000; Rixen et al., 2002) by estimates of the global mean carbonate carbon export (Table 1).

Correspondence to: T. Rixen
(trixen@uni-bremen.de)

Table 1. Contribution of carbonate-producing organism to the pelagic marine carbonate production.

	%	10^{15} g C	References
Total carbonate production	100	0.60–0.86	Milliman and Droxler (1996)
Foraminifera	23–56	0.14–0.48	Schiebel (2002)
Pteropods	∼10	0.06–0.09	Schiebel (2002)*
Coccolithophorids	4–38	0.02–0.33	Schiebel (2002)*

* and references therein.

Possible effects of changing Redfield and rain ratios on the atmospheric CO_2 concentration were quantified using GCMs. It was estimated that an increase of the C/P ratio by 30% (122:1 to 158.6:1) could lower the atmospheric CO_2 concentration by ∼72 ppm (Heinze et al., 1991). A doubling of the global mean rain ratio from 4 to 8 could reduce the atmospheric CO_2 concentration by 28.5 ppm (Heinze et al., 1991), and raising the rain ratio from 5 to 16.6 could, however, reduce the atmospheric CO_2 concentration by 70 ppm (Archer et al., 2000). These changes explaining a major proportion of the glacial/interglacial variation of the atmospheric CO_2 concentration were achieved by assuming that diatoms outcompete the carbonate-producing coccolithophorids and drive the export production. Due to such a competition the rain ratio is directly linked to biogenic opal production in some models used to study the feedback impact of the carbonate production in the ocean on increasing CO_2 concentrations in the atmosphere (Heinze, 2004).

Since diatom growth is believed to be limited by the availability of silicon at lower latitudes (Dugdale and Wilkerson, 1998; Rixen et al., 2000), changes of the global silicon cycle and re-organisation of the marine silicon cycle were proposed as being possible mechanisms to fertilise lower latitudes with silicon during glacial times (Froelich et al., 1992; Harrison, 2000; Conley, 2002; Ridgwell et al., 2002). The re-organisation of the marine silicon cycle is suggested to be triggered by an enhanced eolian iron input lowering the Si/N uptake ratio of diatoms in the Southern Ocean and, subsequently, enhancing the silicon export from higher to lower latitudes (Matsumoto and Sarmiento, 2002).

In addition to coccolithophorids competing with diatoms, there are also carbonate-producing heterotrophs like foraminifera and pteropods which feed on diatoms. In the Arabian Sea sediment trap experiments showed that coccolithophorids contribute only <15% to the carbonate export into the deep sea and that the peak flux of foraminifera into the deep sea coincides with that of diatoms during the highly productive upwelling season (Haake et al., 1993b, 1993a; Zeltner, 2000). This suggests strongly that effects of foraminifera and pteropods on the rain ratio should be taken into consideration, as these organisms are important or even the main carbonate producer in the ocean (Table 1).

The total fluxes of calcium carbonate and organic carbon measured by deep moored sediment traps in the Arabian Sea (Lee et al., 1998; Honjo et al., 1999; Rixen et al., 2002) and ratios between calcium carbonate dissolution and organic carbon remineralization in the water column (Hupe and Karstensen, 2000) have been used to calculate rain ratios (Rixen et al., 2005). In this study these calculated rain ratios ranging between 2 and 3.5 will be compared with rain ratios derived form total dissolved inorganic carbon concentrations (DIC), total alkalinity (TA), and CO_2 partial pressure differences ($\Delta p CO_2$) between the atmosphere and surface water (Goyet et al., 1998b, 1999; Millero et al., 1998). Furthermore plankton counts (Garrison et al., 2000; Schiebel et al., 2004) will be evaluated in conjunction with nutrient (Morrison et al., 1998) and iron concentrations (Measures and Vink, 1999) in order to study factors influencing shifts in the planktonic community structure and associated changes of the composition of sinking particles.

2 Study area

The Arabian Sea is strongly influenced by the Asian monsoon. This climatic feature is driven by the sea-level pressure difference between the Asian landmass and the Indian Ocean (Ramage, 1971, 1987). During the boreal winter the sea level pressure over Asia exceeds that over the Indian Ocean due to a stronger cooling of the landmass. Following the pressure gradient and deflected by the Coriolis force, the wind blows from the NE (NE monsoon) over the Arabian Sea. This situation reverses when the summer heating of the Asian landmass leads to the formation of one of the strongest atmospheric lows on Earth. This low attracts the SE trade winds, and after crossing the equator the former SE winds blow as SW winds over the Arabian Sea due to associated changes of the Coriolis force. The SW winds (SW monsoon) form a tropospheric jet (Findlater Jet) extending almost parallel to the Arabian coast (Fig. 1, Findlater, 1977; Rixen et al., 1996). The monsoon winds and the deserts surrounding the western and northern parts of the Arabian Sea lead to dust inputs into the Arabian Sea, which are among the highest in the world ocean (Tegen and Fung, 1994, 1995).

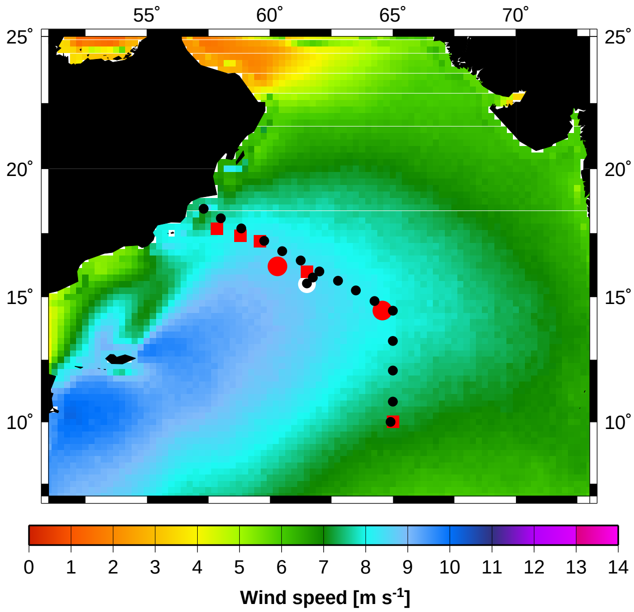

Fig. 1. Mean SW monsoon wind speeds over the Arabian Sea during the SW monsoon. Data are obtained from Rixen et al. (1996). Red squares indicate the U.S. JGOFS (Honjo et al., 1999) and the red circles the long-term Indo/German sediment trap sites in the western and central Arabian Sea (Rixen et al., 2002). The white circle indicate the central Arabian Sea surface mooring location (ONR, Dickey et al., 1998), and the black circles show the U.S. JOGFS water sampling sites (Morrison et al., 1998).

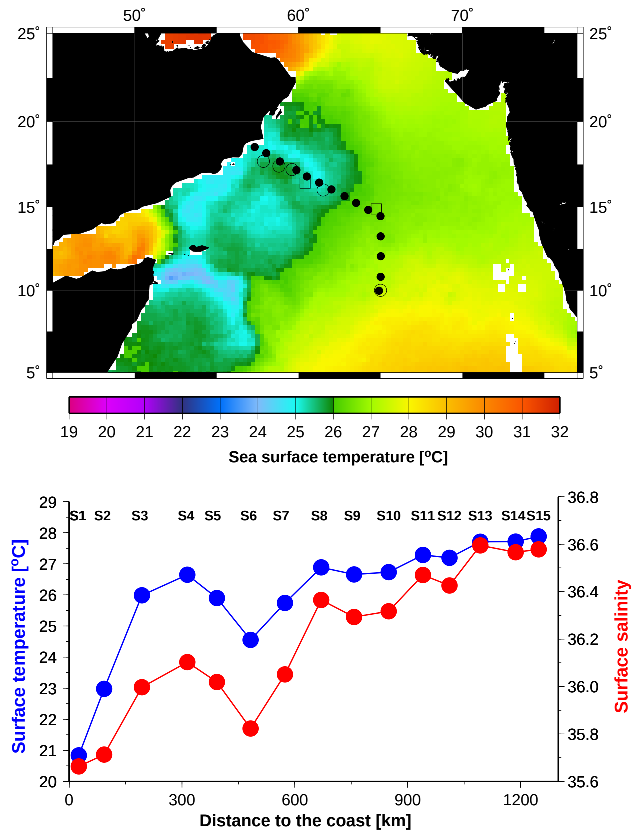

Fig. 2. Upper panel: Mean satellite-derived sea surface temperatures during the cruise ttn49. Data are obtained from Physical Oceanography Distributed Active Archive Center at Jet Propulsion Laboratory, California Institute of Technology). Lower panel: Surface temperatures and salinity averaged for the depth of the mixed layer (data are from the U.S. JGOFS database: http:/usjgofs.whoi.edu/jg/dir/jgofs/arabian/) at each sampling site (S1 to S15).

Biological productivity within the Arabian Sea is determined by the interplay between the euphotic zone and mixed layer depth (MLD), whose deepening is caused by winter cooling and wind mixing (Rixen et al., 2002). The interplay between the euphotic zone and the MLD regulating the availability of light and nutrients is well known from the temperate ocean. In the Arabian Sea this leads to early and late NE monsoon blooms. During the SW monsoon the Findlater Jet creates one of the most productive upwelling areas in the ocean (Antoine et al., 1996) and a hot spot for CO_2 emission along the Arabian coast (Körtzinger et al., 1997; Goyet et al., 1998b, 1998a; Sabine et al., 2000). Diatom blooms are common during the later phases of the NE and SW monsoon (Haake et al., 1993b; Rixen et al., 2000).

3 Data base, methods and results

Nutrients, DIC, TA, temperature, and salinity profiles measured at the sampling sites S1–S15 during the U.S. JGOFS cruises ttn49 (18 July 1995–13 August 1995) and ttn50 (14 August 1995–13 September 1995) were obtained from the U.S. JGOFS database (Figs. 1, 2). The mixed layer depth was defined as the depth at which a pronounced temperature decrease and nutrient increase occurred within profiles. Subsequently all data were averaged for the mixed layer depth (Table 2). The resulting mean mixed layer temperatures and salinities increase generally from the coastal upwelling zone towards the open ocean (Fig. 2). During both cruises slightly reduced temperatures and salinities occurred between stations S5 and S7, approximately 500 km offshore. As shown by satellite-derived SSTs charts (Fig. 2), this anomaly was associated with the filament that extended almost parallel to the transect, perpendicular to the coast towards the open Arabian Sea. Filaments are cold water structures caused by an accelerated advection of upwelled water. While moving offshore the upwelled water get mixed with the warmer and saltier surface water that was formed during the preceding oligotrophic intermonsoon season (Fischer et al., 2002; Weller et al., 2002). Mixing of two water masses is indicated by a linear correlation between temperature (T) and salinity (S) if latent and sensible heat fluxes between ocean and atmospheres are negligible. Temperature und salinity (T/S) data derived from the sampling sites along the Oman transect are not correlated (Fig. 3) and T/S data obtained from

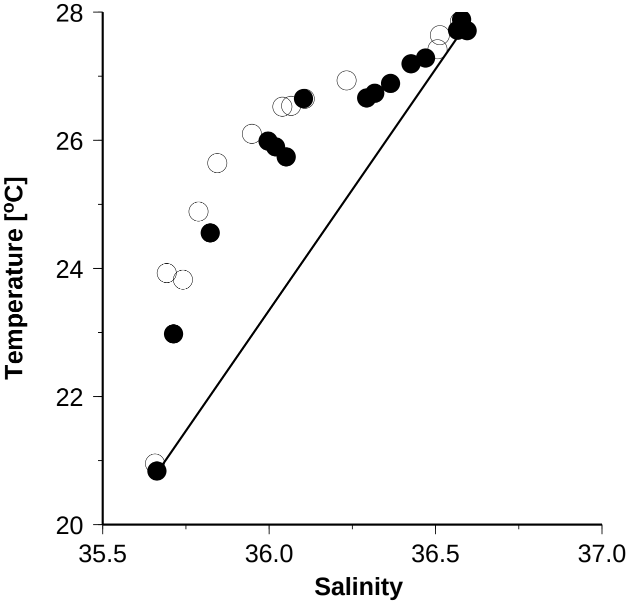

Fig. 3. Salinity versus temperature. Salinities and temperatures were measured during cruise ttn49 (open circles) and ttn50 (black circles) and averaged for the depth of the mixed layer (data are from the U.S. JGOFS database). The black line connects the data collected at the sites S1 and S2.

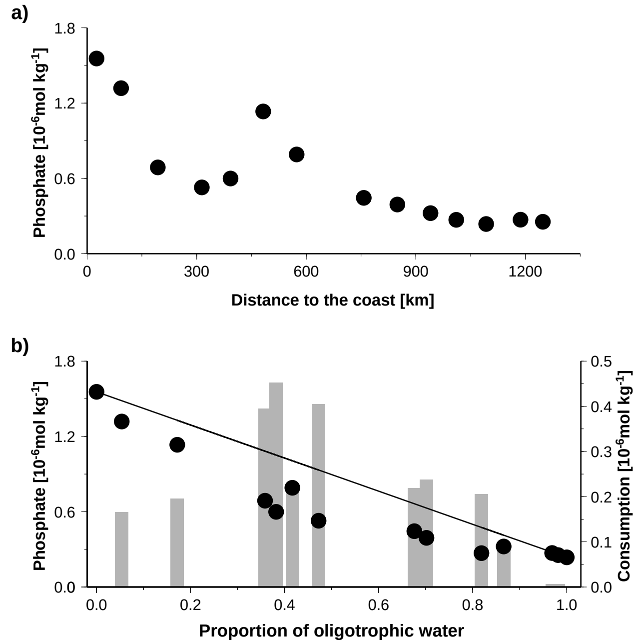

Fig. 4. **(a)** Phosphate concentration measured during cruise ttn49 and averaged for the depth of the mixed layer versus the distance to the coast (data are from the U.S. JGOFS database). **(b)** Mean phosphate concentration (black circles) and the mixing line (black line) versus the proportion of oligotrophic water. Bars reveal the difference between the measured phosphate concentration and the phosphate concentration indicated by the mixing line. This difference is regarded as biological consumption.

the sites S2–S14 deviate from the line (mixing line) that connects T/S data obtained from the sampling site S1 and S15. In order to calculate energy fluxes required to explain these deviations from the mixing line (ΔSST) the time during which the surface water was in contact with the atmosphere must be known. The ages of the surface water can be calculated at each sampling site by dividing the distance to the coast by the mean advection velocity and considering that the upwelled water was already a few days old prior to it left the coast. Since the lower temperatures and the reduced salinity indicate an accelerated advection of upwelled water within the filament an age correction has been applied. The distance from the coast towards the most offshore station (S13) and the station closest to the coast (S1) is ~1100 km and ~26 km, respectively. At these two stations the salinity was 36.6 and 35.7 (Table 2). Based on these two points defined by the distance to the coast and the salinity a linear regression was developed which allowed us to derive corrected distances from the salinity measured at each sampling site (distance [km]=1135.1$\times$Salinity$-$40451.8). The time since the water mass was in contact with the atmosphere was obtained by dividing the corrected distance by the mean advection velocity ranging between 0.2 and 0.8 m s^{-1} (Rixen et al., 2000). Additionally it was assumed that coastally upwelled water was already 4 days old prior to it left the coast. The energy fluxes required to explain ΔSST have been calculated as follows: ($\rho\times$MLD$\times$Cp$\times\Delta$SST)/(age of the water), whereas "ρ" is the sea water density in "kg m^{-3}", MLD is the mixed layer depth in "m", "cp" is the specific heat of the water (~3980 J kg^{-1} K^{-1}), ΔSST and the age of the water are given in "°C" and seconds, respectively. The calculated data show that a heat flux of 90 to 584 W m^{-2} could have caused the ΔSST at sampling site S7 (Table 3). Energy fluxes of 150 to 200 W m^{-2} determined at the U.S. JGOFS surface mooring site which is close to S7 (Weller et al., 1998) fall within this range implying that heat fluxes could have caused ΔSST at station S7 and most probably also at the other water sampling sites for which no data on heat fluxes are available.

Latent heat fluxes do not affect the relationship between salinity and nutrient concentrations as changes in the amount of water in the mixed layer increase both the salinity and the nutrient concentration. Since in addition to that salinity and nutrient concentration are unaffected by sensible heat flux, salinity instead of temperature was used to define the end-members and to calculate the mixing ratios "a" and "b" within the two-end-member mixing analysis at sampling sites S1–S13 (Salinity$_{S1-S13}$=a$_{S1-S13}\times$Salinity$_{\text{upwelled water}}$+b$_{S1-S13}$ Salinity$_{\text{oligotrophic water}}$, whereas a$_{S1-S13}$+b$_{S1-S13}$=1). Station S1 was defined as the upwelling and station S13 as the oligotrophic end-member because there are hardly any discernible variations in the salinity between stations S13,

Table 2. Station number, position, distance between the station and the coast, mixed layer depth, mean mixed layer temperature, salinity, phosphate, total inorganic nitrogen , silicon and total inorganic carbon concentration, mean total alkalinity and partial pressure difference between the atmosphere and the ocean. Missing data are indicated by −99.00. The position was obtained by averaging the position of all available hydrographic casts at one sampling sites.

St.	Lon. [° E]	Lat. [° N]	Distance [km]	MLD [m]	Temp. [C]	Sal. [psu]	PO_4	TN	Si	DIC	TA μeq./kg	ΔpCO_2 μatm
							———[μmol/kg]———					
Cruise ttn49												
S1	57.32	18.52	25.73	10.00	20.84	35.66	1.55	17.40	9.23	2146.50	2338.60	−299.09
S2	58.03	18.16	93.01	18.00	22.98	35.71	1.32	15.40	7.64	2111.43	2329.18	−222.65
S3	58.86	17.67	193.58	53.00	25.99	36.00	0.69	5.58	3.13	2046.65	2349.28	−99.37
S4	59.87	17.17	313.98	42.00	26.65	36.10	0.53	4.12	2.73	2044.78	2348.66	−83.25
S5	60.51	16.79	392.79	48.00	25.90	36.02	0.60	4.81	2.51	2042.92	2348.80	−89.41
S6	61.25	16.43	482.12	40.00	24.55	35.82	1.13	12.16	5.59	2091.47	2340.20	−159.56
S7	62.00	16.03	573.55	34.00	25.74	36.05	0.79	7.25	3.55	2056.73	2350.63	−116.40
S8	62.81	15.64	669.95	75.00	26.89	36.37	−99.00	1.52	1.80	2030.58	2369.00	−57.44
S9	63.51	15.23	757.38	82.00	26.66	36.29	0.44	2.01	1.25	2035.04	2362.73	−54.62
S10	64.25	14.82	849.37	83.00	26.73	36.32	0.39	0.96	1.16	2028.16	2366.69	−39.80
S11	65.00	14.44	940.11	75.00	27.28	36.47	0.32	0.51	0.99	2024.41	2375.23	−27.76
S12	65.00	13.24	1010.75	84.00	27.19	36.43	0.27	0.04	0.54	2020.13	2373.47	−27.38
S13	65.01	12.05	1092.72	108.00	27.71	36.60	0.24	0.17	0.69	2018.74	2382.50	−19.72
S14	65.00	10.81	1186.65	104.00	27.72	36.57	0.27	0.29	1.10	2020.96	2381.27	−23.93
S15	64.91	9.97	1247.93	95.00	27.88	36.58	0.25	0.40	1.19	2017.80	2381.40	−27.45
Cruise ttn50												
S1	57.30	18.50	23.26	14.00	20.95	35.66	1.66	19.42	11.18	−99.00	−99.00	−99.00
S2	58.04	18.09	96.34	10.00	23.93	35.69	1.32	15.09	5.71	−99.00	−99.00	−99.00
S3	58.85	17.67	192.68	20.00	23.82	35.74	1.07	11.50	1.99	−99.00	−99.00	−99.00
S4	59.77	17.18	303.75	25.00	24.89	35.79	0.96	9.62	1.51	−99.00	−99.00	−99.00
S5	60.50	16.80	392.48	52.00	25.64	35.84	0.85	8.38	1.12	−99.00	−99.00	−99.00
S6	61.25	16.43	481.32	52.00	26.65	36.11	0.53	3.15	0.97	−99.00	−99.00	−99.00
S7	61.98	16.01	573.00	50.00	26.52	36.04	0.59	3.84	1.49	−99.00	−99.00	−99.00
S8	62.77	15.64	666.57	48.00	26.10	35.95	0.76	6.52	1.70	−99.00	−99.00	−99.00
S9	63.50	15.25	756.05	74.00	26.54	36.07	0.57	3.84	2.42	−99.00	−99.00	−99.00
S11	65.00	14.44	940.20	75.00	26.93	36.23	0.41	1.22	0.73	−99.00	−99.00	−99.00
S13	65.00	12.05	1091.55	102.00	27.42	36.51	0.34	0.31	0.59	−99.00	−99.00	−99.00
S14	65.00	10.80	1186.62	100.00	27.64	36.51	0.32	0.09	0.42	−99.00	−99.00	−99.00
S15	64.90	9.97	1247.66	84.00	27.85	36.57	0.30	0.13	0.27	−99.00	−99.00	−99.00

14 and 15 (Table 2). A mixing ratio "b" of zero indicates pure upwelled water whereas a mixing ratio "b" of one implies that no upwelled water is present. The mixing ratios "a" and "b" determined for each station and the mean nutrient concentration calculated at the station S1 and S13 (see Table 2) were subsequently used to calculate a mixing line ($\text{Phosphate}_{\text{S1}-\text{S13mixing}}=\text{a}_{\text{S1}-\text{S13}}\times\text{Phosphate}_{\text{S1}}+\text{b}_{\text{S1}-\text{S13}}$ Phosphate_{S13}; Fig. 4b). The mixing line represents the concentration that could be expected if mixing were the only factor controlling the nutrient concentration. Deviations of measured phosphate, inorganic nitrogen, and silicon concentrations from the mixing line can be attributed to biological consumption. In order to determine error ranges of the derived biological consumption caused by analytical methods, a relative percentage error of 0.5% and 0.012% of nutrient and salinity data (U.S. JGOFS data base documentation) was considered. Within these error ranges random errors were produced by applying the standard fortran 77 random number generator (F77-RNG). Subsequently, the mixing analysis was performed 500 times by using the produced errors. The mean ratios of inorganic nitrogen and phosphate consumptions (N/P ratios) vary between ∼7 and 24 (Fig. 5b) and fall within the range of N/P ratios determined in marine particulate matter and phytoplankton (∼3–34, Geider and La Roche, 2002; Klausmeier et al., 2004). The resulting standard deviations of the N/P ratios range between 0.1 and 0.4.

The DIC and TA data were treated in the same way as nutrient data, but prior to calculating the biological consumption the DIC concentrations were corrected for CO_2 emission. The CO_2 emission into the atmosphere have

Table 3. Sampling site, the mean mixed layer temperature (determined), the temperature as suggested by the mixing line indicate in Fig. 4 (expected), the difference between the mixed layer temperature and the expected temperature (ΔSST), and energy fluxes required to explain the temperature deviation. The energy flux has been calculated by assuming a mean advection velocity of 0.8 and $0.2\,\mathrm{m\,s^{-1}}$.

Sampling site	Temperature [°C] determined	expected	deviation	Energy fluxes [$\mathrm{W\,m^{-2}}$] $0.2\,\mathrm{m\,s^{-1}}$	$0.8\,\mathrm{m\,s^{-1}}$
ttn 49					
S12	27.19	26.86	0.32	76.700	23.298
S11	27.28	27.20	0.08	16.303	4.909
S10	26.73	26.02	0.70	183.139	57.077
S9	26.66	25.84	0.82	214.771	67.379
S8	26.88	26.39	0.49	109.286	33.650
S7	**25.74**	**23.97**	**1.76**	**261.963**	**90.695**
S6	24.55	22.22	2.33	623.791	271.435
S5	25.89	23.73	2.16	477.645	168.688
S4	26.65	24.37	2.27	386.403	130.107
S3	25.98	23.56	2.42	612.288	219.543
S2	22.97	21.37	1.60	259.434	151.544
ttn50					
S11	26.93	25.37	1.55	399.021	127.506
S9	26.53	24.09	2.44	772.361	265.124
S8	26.10	23.18	2.91	725.146	270.388
S7	**26.52**	**23.89**	**2.63**	**584.430**	**203.671**
S6	26.64	24.40	2.24	468.718	157.517
S5	25.64	22.38	3.26	1081.012	454.687
S4	24.88	21.95	2.93	534.635	249.007
S3	23.82	21.59	2.23	369.189	194.683
S2	23.92	21.21	2.71	261.293	168.481

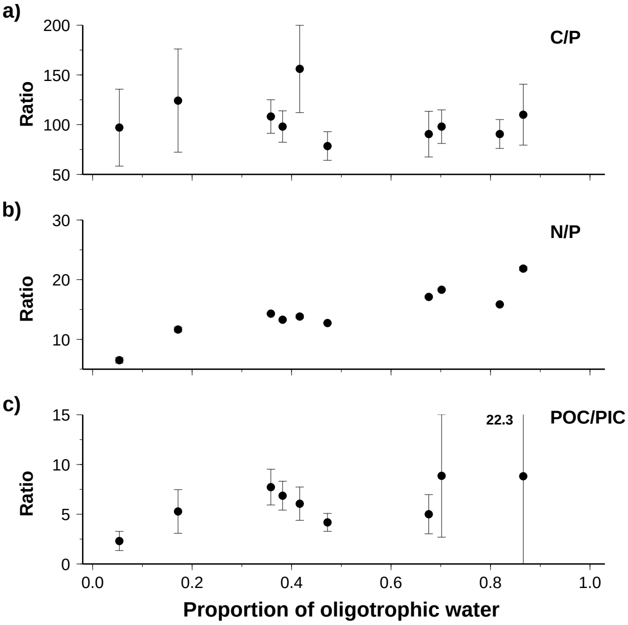

Fig. 5. **(a)** C/P, **(b)** N/P and **(c)** rain (POC/PIC) ratios versus the proportion of oligotrophic water. Error bars are calculated as described in the text. The number in panel (c) indicates the rain ratio at the sampling site S11 which is not plotted as it is out of scale.

been derived from the $\Delta p\mathrm{CO_2}$ data published for each water sampling site in the U.S. JGOFS database (Table 2). The required wind-dependent gas transfer velocity "k" was calculated using eight different formulations (Liss and Merlivat, 1986; Wanninkhof, 1992; Wanninkhof and McGillis, 1999; Nightingale et al., 2000; Feely et al., 2001). Satellite-derived wind speeds (see Fig. 1) were taken from Rixen et al. (1996). The standard deviation and the resulting mean CO_2 emission at each sampling site along the transect are given in Fig. 6. In order to estimate the amount of CO_2 that escaped from the surface water, the CO_2 emissions have been multiplied by the age of the water which has been was calculated by using a mean advection velocity of $0.6\,\mathrm{m\,s^{-1}}$. The resulting mean CO_2 loss was subtracted from the amount of DIC held in the mixed layer. A further correction for the penetration of anthropogenic CO_2 was neglected because of the short time scale covered by the cruises. The CO_2-corrected DIC and the TA consumption ($\mathrm{DIC_{consumption}}$, $\mathrm{TA_{cons.}}$) have been used for differentiating between the net organic carbon production ($\mathrm{POC_{production}}$) and the precipitation of calcium carbonate ($\mathrm{PIC_{precipitation}}$), according to the equations:

$$\mathrm{DIC_{consumption}}=\mathrm{POC_{production}}+\mathrm{PIC_{precipitation}} \tag{1}$$

$$\mathrm{PIC_{precipitation}}=(\mathrm{TA_{cons.}}+\mathrm{POC_{production}}\times 0.15)/2 \tag{2}$$

The factor 0.15 accounts for the increase of TA during the production of organic matter, and the factor 2 due to the fact that for each mole of carbonate precipitated from the sea water TA decreases by two units (Broecker and Peng, 1982; Zeebe and Wolf-Gladrow, 2001). With two equations and two unknowns the production of organic carbon ($\mathrm{POC_{production}}$) can be determined as follows:

$$\mathrm{POC_{production}}=(\mathrm{DIC_{corrected}}-\mathrm{TA_{cons.}}/2)/1.08 \tag{3}$$

Error ranges were determined by producing "analytical" errors artificially by applying the F77-RNG within the range of the standard deviation given for the determination of DIC concentrations ($\pm 1.2\ 10^{-6}\,\mathrm{mol\,kg^{-1}}$) and TA ($\pm 3.2\ 10^{-6}$eq. $\mathrm{kg^{-1}}$ Millero et al., 1998; U.S. JGOFS data base documentation). Subsequently the errors were used to recalculate the POC and PIC production 500 times for each of the different gas transfer velocity coefficients cited above. The resulting mean C/P and rain ratios and their standard deviations are given in Fig. 5a. The mean C/P uptake ratios vary between 80 and 150 and are well within the range of published C/P ratios observed in marine particulate matter and phytoplankton. The same holds true for the rain ratios which vary between $\sim$2.3 and $\sim$8.1 except at station S11

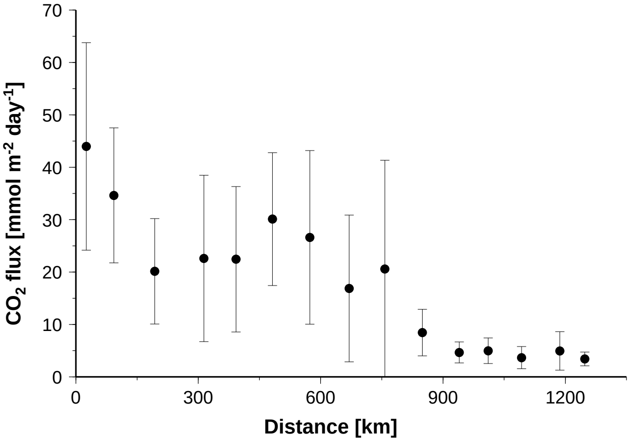

Fig. 6. Mean CO_2 emission derived from ΔpCO_2 data obtained from the U.S. JGOFS data, satellite-derived wind speeds and the different gas transfer velocity coefficients "k" versus the distance to the coast. Error bars indicate the standard variation of results derived from the different wind speed data sets and the different methods to calculate "k".

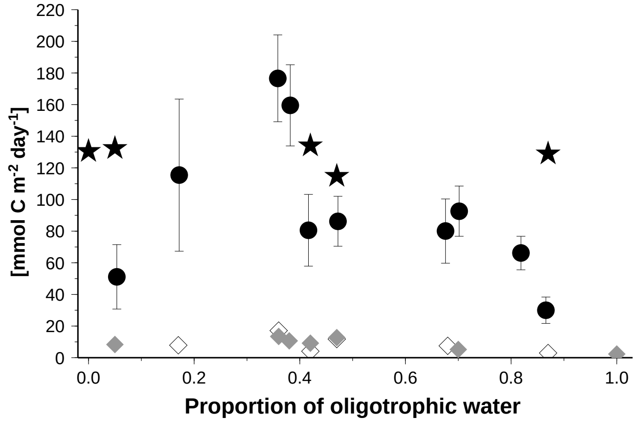

Fig. 7. Primary production rates (stars), export production rates derived from ^{234}Th measurements (open diamonds; Buesseler et al., 1998), and sediment trap data (grey diamonds; Rixen et al., 2003). Organic carbon (new) production calculated from the DIC and TA uptake is indicated by black circles.

where the rain ratio is 22.3 (Fig. 5c). However, due to the low carbon consumption the standard deviation at the sampling sites S10–S12 (proportion of oligotrophic water >0.7) are so high that these data have to be treated with caution within the following discussion.

In order to calculate the new production rates (Dugdale and Goering, 1967; Eppley and Peterson, 1979) the $POC_{production}$ (see Eq. 3) was integrated over the depth of the mixed layer and subsequently divided by the age of the upwelled water. The comparison with primary and export production rates measured at the same time and at the same stations (Buesseler et al., 1998) show that the resulting new carbon production rates are lower than the primary production rates, as expected (Fig. 7). Since new production exceeds export production rates it is assumed that the biomass is growing in the mixed layer but under different environmental conditions.

New production rates which are consistent with published data on primary and export production rates and reliable rain and Redfield ratios suggest that our approach is suitable for studying biogeochemical processes in the Arabian Sea during the upwelling season. In the following discussion the results obtained by our mixing analysis will, furthermore, be linked to plankton counts and sediment trap data in order to investigate factors influencing changes in the planktonic community structure and associated impacts on the rain ratio.

4 Discussion

4.1 Diatom blooms

The shoaling of the mixed layer and enhanced organic carbon flux measured in the deep sea reveal that the cruise ttn49 and the cruise German JGOFS cruise M32/5 took place at the beginning of the upwelling season in the open western Arabian Sea (Fig. 8). On month later during the cruise ttn50 the high organic carbon fluxes indicate the peak upwelling season. At this time plankton counts (Garrison et al., 2000) show that diatoms dominate the planktonic community from approximately 100 to 400 km offshore (Fig. 9b). Flagellates succeed diatoms in the central Arabian Sea after silicon concentrations in the surface water reach their oligotrophic intermonsoon value of $\sim 2\,\mu\text{mol kg}^{-1}$, (compare Figs. 9b and d). Plankton growth rates generally decrease with decreasing nutrient concentrations after the latter falls below a certain threshold (Lalli and Parsons, 1993). Assuming that such a threshold is close to a silicon concentration of $\sim 2\,\mu\text{mol kg}^{-1}$ diatom growth rates falling below the high grazing rates (Smith et al., 1998) could explain the declining diatom bloom in the open western Arabian Sea where silicon in the surface water is not consumed. This observation confirms experimental data suggesting a silicon-threshold of $\sim 2\,\mu\text{mol kg}^{-1}$ for the dominance of diatoms within the planktonic community (Egge and Aksnes, 1992). Near the coast, at silicon concentration of $\sim 11\,\mu\text{mol kg}^{-1}$ the relatively low contribution of diatoms to the planktonic community (Fig. 9b, d) has been attributed to intense grazing by copepods slowing down the development of diatom blooms in the coastal region off Oman (Smith, 2001). During the early phase of the upwelling season the abundance of diatoms decreased drastically close to the Oman coast as shown by plankton counts

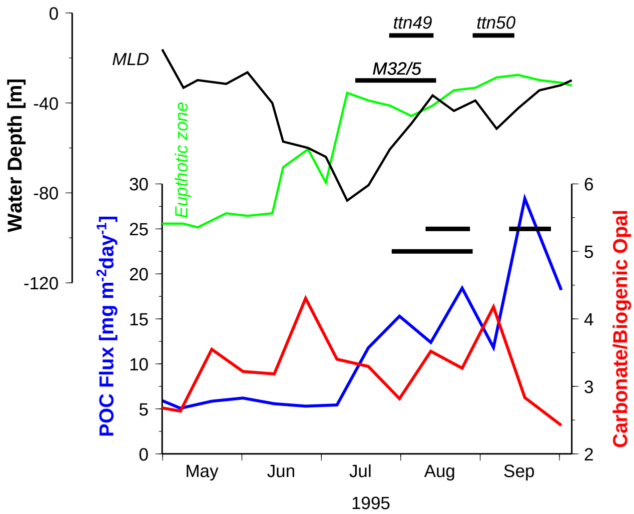

Fig. 8. Depth of the mixed layer (MLD black line) and of the euphotic zone (1% light level; green line) determined at the ONR mooring site. Data was redrawn from (Dickey et al., 1998). The MLD represents the water-depth at which the temperature is 1°C lower than at the surface. The organic carbon fluxes (black line) and carbonate/biogenic opal ratios (red line) measured in the western Arabian Sea at the long-term Indo/German sediment trap site (WAST) at 3000 m water-depth. The horizontal black lines show the time during which the cruises M32/5 have been carried out and the cruises ttn49 and 50 have been performed along the transect off Oman in the western Arabian Sea. The other horizontal lined indicate the time at which the measured surface data could be reflected in the deep ocean. A delay of 14 days has been added to original dates.

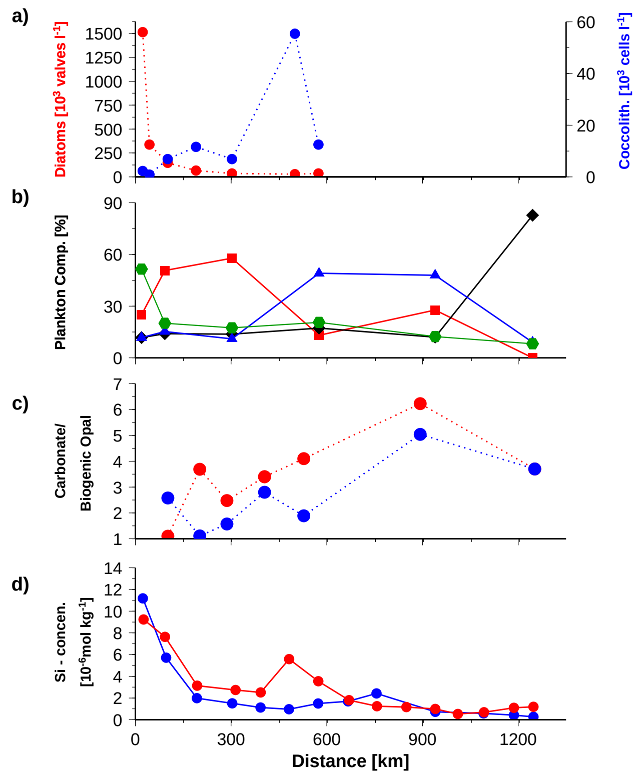

Fig. 9. **(a)** Number of diatom valves and coccolithophorid cells (Schiebel et al., 2004) **(b)** contribution of nanoplankton (green), diatoms (red), flagellates (blue) and cyanobacteria (black) to the biomass of photoautotrophic plankton (Garrison et al., 2000), **(c)** Carbonate biogenic opal ratios (blue – peak upwelling season; red – onset of the upwelling season) derived from deepest sediment traps deployed at the U.S., JGOFS and Indo/German sediment trap site (see Figs. 1 and 2) **(d)** silicon concentrations (blue – ttn50, red – ttn49) versus the distance to the coast. The sediment traps have been deployed at water-depth ranging approximately between 2500 and 3500 m except near the coast the sediment trap was deployed at a water-depth of ∼1000 m.

(Fig. 9a, Schiebel et al., 2004). This decline is accompanied with a transition from a *Chaetoceros* dominated diatom assemblage near the coast to one dominated by *Nitzchia bicapitata* further offshore. The decline and the associated transition of the diatom assemblage has been linked to decreasing nutrient concentrations and intense grazing (Smith, 2001; Schiebel et al., 2004).

The results obtained by the plankton counts agree with those derived from deep moored sediment traps and our mixing analysis showing silicon consumption and carbonate biogenic opal ratios which are lower and higher, respectively, during the early than during the later phase of the upwelling season in the open western Arabian Sea (Figs. 9c, 10a). Vice versa, near the coast carbonate biogenic opal ratios reveal a higher contribution of diatoms to the exported matter during the early than during the later phase of the upwelling season (Fig. 9c). This seems to be caused by the export of the declining diatom bloom during the early phase of the upwelling season (Fig. 9a) and the delayed development of the diatom bloom one month later (Fig. 9b).

4.2 The role of iron for the development of diatom blooms

Iron enrichment experiments in the coastal upwelling system off California revealed that iron fertilization favours the growths rates of *Chaetoceros* and other diatoms but leads to the formation of thinner shells as indicated by a low uptake of silicon relative to nitrogen (Hutchins and Bruland, 1998). The iron concentration in the diatom dominated open western Arabian Sea range between 0.5 and 1 nmol l^{-1} during the cruise ttn50 and reach values of >2 nmol l^{-1} during the cruise ttn49 near the coast (Fig. 10b). Off California an increase in the iron concentration from 0.5 to 2.5 halves Si/N uptake ratio (Hutchins and Bruland, 1998). Assuming a similar impact of iron on the Si/N uptake off Oman suggests that *Chaetoceros* blooming during the onset of the upwelling season near the coast off Oman might built thinner

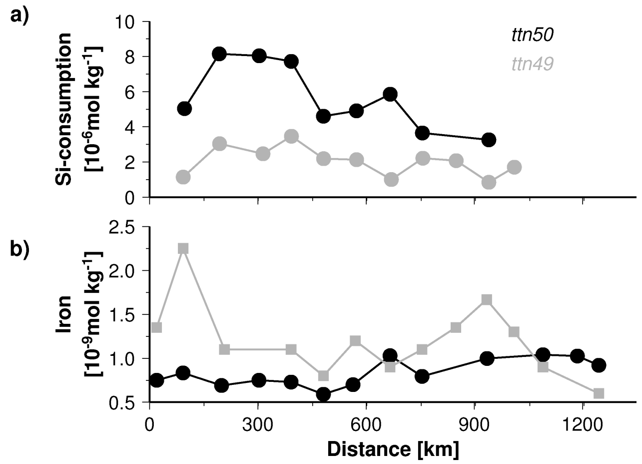

Fig. 10. **(a)** Silicon consumption, **(b)** iron concentration versus the distance to the coast during the cruises ttn49 and 50.

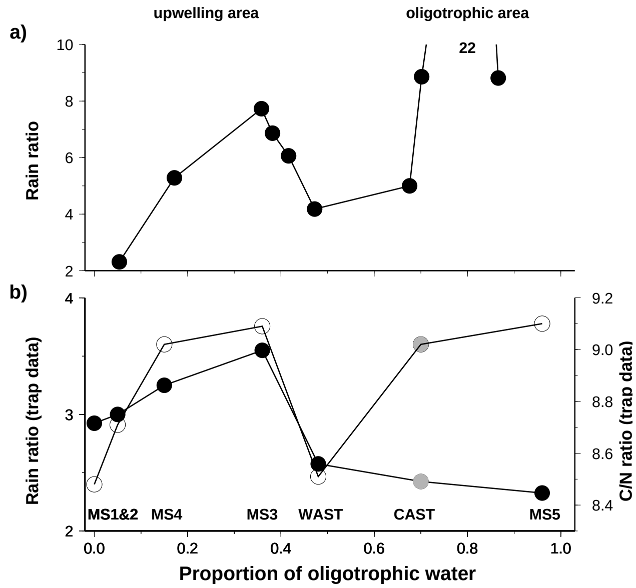

Fig. 11. **(a)** Rain ratios and silicon consumption derived from the mixing analysis versus the proportion of oligotrophic water (same data as shown in Figs. 5 and 10a). **(b)** Rain (black circles) and C/N ratios (open circles) derived from sediment traps versus the proportion of oligotrophic water data. The rain ratios are mean SW monsoon values and have been derived from trap data (Rixen et al., 2005). The C/N ratios obtained from deepest trap deployed at each mooring site have been averaged for the period of the cruise ttn4. The proportion of oligotrophic water was determined by adjoining to them the closest water-sampling site during the cruise ttn49. Since lateral advection has to be considered additionally, not the closest station was used but its neighbour station to the west (coast). The grey circles indicate long-term mean rain and C/N ratio obtained from the Indo/German sediment trap site in the central Arabian Sea (CAST), but it does not include data from the SW monsoon 1995, due to an instrumental error.

shells than diatoms growing a month later in same region but in water revealing lower iron concentrations. The extremely strong diatom shell is an important protection against predators (Hamm et al., 2003). Since enhanced iron concentrations lead to the formation of thinner shells it is suggested that copepode grazing is favoured in iron-enriched environments. An iron-favoured grazing could explain the decline of the near shore diatom bloom during the onset of the upwelling season (Fig. 9a). On the other hand a less efficient grazing due to lower iron concentrations (Fig. 10b) and thicker shells could slow down but do not prevent the development of a large diatom bloom during the later phase of the upwelling season (Fig. 9b) at which the silicon concentrations are almost equal to those during early phase of the upwelling season (Fig. 10d).

4.3 Rain ratios

Apart from one exception as discussed before the rain ratios derived from mixing analysis range between $\sim$2.3 and 8.1 and are generally higher than those obtained from sediment trap data (2–3.5, Fig. 11). The rain ratios derived from the sediment trap data have been adjusted to a water-depth of 100 m whereas the mixed layer depth is $<$100 m in the western Arabian Sea (Table 1). POC/PIC ratios tend to decrease within increasing water depth because the decomposition of organic matter is faster than the dissolution of carbonates in the upper water column. Consequently, the difference between rain ratios derived from sediment trap data and the mixing analysis could be caused by differences in the water-depth. Moreover, one should consider that sediment trap data represent a larger area and a longer time interval than data derived form nutrient profiles obtained at a specific site within a relatively short period of time.

However, rain ratios obtained from sediment trap data and the mixing analysis reveal a similar trend in the upwelling region characterized by a proportion of oligotrophic water (pow) $<$0.6 (Fig. 11). Near the upwelling centres (pow $<$0.35) the rain ratios increase with an increasing proportion of oligotrophic water until they reach a maximum at a pow of $\sim$0.35. This increase is accompanied with an enhanced silicon consumption (Fig. 10a) indicating a slight recovery of the diatom (*Nitzchia bicapitata)* bloom after the dramatic decline of *Chaetoceros* dominated diatom bloom near the coast during the early upwelling season (Fig. 9a). At the transition between the upwelling dominated area and the more oligotrophic sites the rain ratios decrease by $\sim$30 (sediment trap data) and 45% (mixing analysis). This decline is accompanied with decreasing silicon consumption (Fig. 10a) and during the later phase of the upwelling season also with decreasing contribution of diatoms to the plantonic community structure (Fig. 9b).

The high abundance of coccolithophorids at approximately 450 km offshore (Fig. 9a) occurred in a water mass

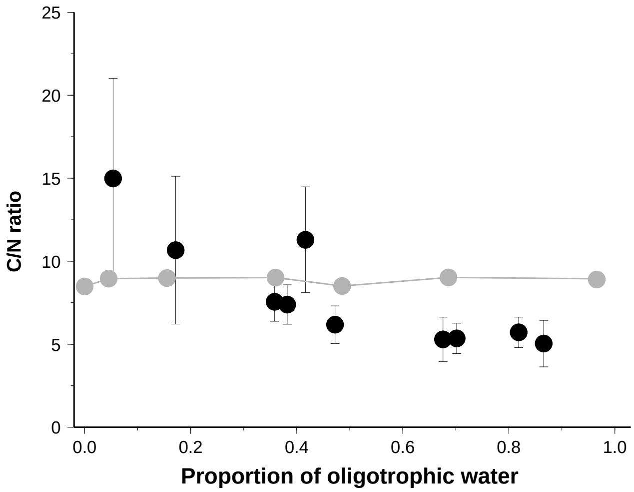

Fig. 12. C/N ratios derived from the mixing analysis (black circles) and sediments traps (grey circles, same data as in Fig. 11b) versus the proportion of oligotrophic water.

which is characterized by a pow of ∼0.2. The associated rain ratio of ∼5 is relatively high (Fig. 11a) and implies in line with sediment trap results that coccolithophorids are only of minor importance for the carbonate export in the Arabian Sea. This in turn implies that changes of the rain ratios as discussed before are mainly caused by variations in the growth and export rates of foraminifera. Enhanced rain ratios associated with even a slightly increased contribution of diatoms in the planktonic community structure could for example results from predators such as copepods competing with foraminifera for diatoms.

High rain ratios seem to characterize the oligotrophic region, in which cyanobacteria dominate the planktonic community (Figs. 11, 9b). These high rain ratios derived from mixing analysis are not mirrored by the sediment trap data which reveal the lowest values in this region (Fig. 11). Since it is generally assumed that cyanobacteria are rapidly remineralized in the upper water column and hardly sink into the deep sea (Karl et al., 1996, 1997) a preferential decomposition of cyanobacterial biomass could explain the difference between the rain ratios derived from the mixing analysis and the those obtained from the sediment trap data. A preferential decomposition of more labile nitrogen containing compounds in the water column (Lee and Cronin, 1982; Wakeham et al., 1997; Lee et al., 2000) is also indicated by C/N ratios which are lower in the organic matter produced in the surface water than those measured in organic matter intercepted by sediment traps in the oligotrophic regions (Fig. 12).

4.4 C/N and C/P ratios

Contrary to the oligotrophic region C/N ratios partly decrease with depth impling a preferential decomposition carbon-enriched material in the upwelling area (Fig. 12). Such carbon-enriched organic matter could be transparent exopolymers (TEP) which are produced by diatoms and foster the formation of fast-sinking marine snow (Passow et al., 1994, 2001). The formation of TEP raises the C/P ratios especially at the end of diatom blooms (Engel et al., 2002) and along the transect at the transition from the upwelling towards the oligotrophic system the CP ratios reveal a drop from values >108 to 78 (Fig. 5a). The huge decrease of the C/P and C/N ratios is not reflected in the C/N ratios of the exported matter in the deep sea which show only a ∼7% decrease at the transition from the upwelling towards the oligotrophic system (Fig. 11b). This implies that the preferential decomposition of TEP-like organic matter in the upper water column reduces the impact of the TEP formation on the Redfield ratio in the exported matter during diatom blooms.

5 Conclusions

The evaluation of data collected during the U.S. and German JGOFS expedition in 1995 suggest that an intense grazing decline and impede the development of large diatom blooms in a silicon-enriched near shore upwelling system off Oman. Within the offshore advecting upwelled water mass a large diatom blooms enhancing the organic carbon export into the deep sea develop only during the later phase of the upwelling period. During the onset of the upwelling season no large diatoms blooms occurs in the open western Arabian Sea, despite increased concentrations of dissolved silicon in the surface water. Enhanced iron concentration due to eolian dust inputs into the offshore advecting upwelled water might have favoured grazing at this time because it leads to the formation of thinner diatom shells. The decrease of the rain ratios during transition from upwelling towards the oligotrophic offshore region seems to be caused by foraminifera competing with diatom-grazing copepods for food. The large variability of Redfield ratios and also of the rain ratios in the oligotrophic region is not reflected in the sediment trap record. This suggests that the decomposition of organic matter in the water columns contributes to the relative uniform global mean Redfield ratio and leads to an underestimation of rain ratios derived from sediment traps records in oligotrophic regions dominated by cyanobacteria.

Acknowledgements. We would like to thank all the scientists, technicians, and officers and their crews of the numerous research vessels as well as the national funding agencies who made the Joint Global Ocean Flux Study in the Arabian Sea possible. Particularly, we would like to appreciate the work of S. Honjo, S. Manganini, T. Dickey, K. Buesseler, C. I. Measures, S. Vink, J. M. Morrison, D. L. Garrison, L. Codispoti, and S. L. Smith which in particular contributed to our study. We would like to thank also C. Lee, S. W. A. Naqvi and T. Pohlmann for helpful discussions. Furthermore, we are grateful to the Federal German Ministry for Education, Science, Research and Technology (BMBF, Bonn) and the German Research Council (DFG, Bonn), the Council of Scientific and Industrial Research (CSIR, New Delhi), and the Department of Ocean Development (DOD, New Delhi) for financial support of the Bilateral Indo/German Program on Biogeochemical Fluxes in the northern Indian Ocean. P. Wessels and W. H. F. Smith are acknowledged for providing the generic mapping tools (GMT), as well as B. Aksen for secretarial assistance.

Edited by: A. Watson

References

Anderson, L. A. and Sarmiento, J. L.: Redfield ratios of remineralization determined by nutrient data analysis, Global Biogeochem. Cycles, 8(1), 65–80, 1994.

Antoine, D., André, J.-M., and Morel, A.: Oceanic primary production – 2. Estimation at global scale from satellite (coastal zone color scanner) chlorophyll, Global Biogeochem. Cycles, 10(1), 57–69, 1996.

Archer, D., Winguth, A. M. E., Lea, D., and Mahowald, N.: What caused the glacial/interglacial atmospheric $p\mathrm{CO}_2$ cycles?, Rev. Geophys., 38(2), 159–189, 2000.

Berger, W. H. and Keir, R. S.: Glacial-Holocene Changes in Atmospheric CO_2 and the Deep-Sea Record, in: Climate Processes and Climates Sensitivity, edited by: Hansen, J. E. and Takahashi, T., Am. Geophys. Union, Washington, 337–351, 1984.

Broecker, W. S. and Peng, T.-H.: Tracers in the sea, Lamont-Doherty Geological Observatory, Columbia University, Palisades, New York, 690 pp., 1982.

Buesseler, K., Ball, L., Andrews, J., Benitez-Nelson, C., Belastock, R., Chai, F., and Chao, Y.: Upper ocean export of particulate organic carbon in the Arabian Sea derived from thorium-234, Deep Sea Research II, 45(10–11), 2461–2487, 1998.

Burkhardt, S., Zondervan, I., and Riebesell, U.: Effect of CO_2concentration on C: N: P ratio in marine phytoplankton: A species comparison, Limnology and Oceanography, 44(3), 683–690, 1999.

Conley, D. J.: Terrestrial ecosystems and the biogeochemical silica cycle, Global Biogeochem. Cycles, 16(4), 68-1–68-8, 2002.

Dugdale, R. C. and Goering, J. J.: Uptake of new and regenerated forms of nitrogen in primary productivity, Limnology and Oceanography, 12, 196–206, 1967.

Dugdale, R. C. and Wilkerson, F. P.: Silicate regulation of new production in the equatorial Pacific upwelling, Nature, 391, 270–273, 1998.

Egge, J. K. and Aksnes, D. L.: Silcate as regulating nutrient in phytoplankton competition, Marine Ecology Progress Series, 83, 281–289, 1992.

Engel, A., Goldtwait, S., Passow, U., and Alldredge, A. L.: Temporal decoupling of carbon and nitrogen dynamics in a mesocosm diatom bloom, Limnology and Oceanography, 47(3), 753–761, 2002.

Eppley, R. W. and Peterson, B. J.: Particulate organic matter flux and planktonic new production in the deep ocean, Nature, 282, 677–680, 1979.

Falkowski, P., Scholes, R. J., Boyle, E., Canadell, J., Canfield, D., Elser, J., Gruber, N., Hibbard, K., Högberg, P., Linder, S., Mackenzie, F. T., Moore III, B., Pedersen, T., Rosenthal, Y., Seitzinger, S., Smetacek, V., and Steffen, W.: The Global Carbon Cycle: A Test of Our Knowledge of Earth as a System, Science, 290, 291–296, 2000.

Feely, R. A., Sabine, C. L., Takahashi, T., and Wanninkhof, R.: Uptake and storage of carbon dioxide in the ocean: The global survey, Oceanography, 14(4), 18–32, 2001.

Findlater, J.: Observational Aspects of the Low-level Cross-equatorial Jet Stream of the Western Indian Ocean, Pageoph., 115, 1251–1262, 1977.

Fischer, A. S., Weller, R. A., Rudnick, D. L., Eriksen, C. C., Lee, C. M., Brink, K. H., Fox, C. A., and Leben, R. R.: Mesoscale eddies, coastal upwelling, and the upper-ocean heat budget in the Arabian Sea, Deep Sea Research Part II: Topical Studies in Oceanography, 49(12), 2231–2264, 2002.

Froelich, P. N., Blanc, V., Mortlock, R. A., and Chillrud, S. N.: River fluxes of dissolved silica to te ocean were higher during glacials: Ge/Si in diatoms, rivers, and oceans, Paleoceanography, 7(6), 739–767, 1992.

Garrison, D. L., Gowing, M. M., Hughes, M. P., Campbell, L., Caron, D. A., Dennett, M. R., Shalapyonok, A., Olson, R. J., Landry, M. R., and Brown, S. L.: Microbial food web structure in the Arabian Sea: a US JGOFS study, Deep Sea Research II, 47(7–8), 1387–1422, 2000.

Geider, R. J. and La Roche, J.: Redfield revisited: variability of C:N:P in marine microalgae and its biochemical basis, European Journal of Phycology, 37, 1–17, 2002.

Goldman, J. C., McCarthy, J. J., and Peavey, D. G.: Growth rate influence on the chemical composition of phytoplankton in oceanic waters, Nature, 279, 210–214, 1979.

Goyet, C., Millero, F. J., O'Sullivan, D. W., Eischeid, G., McCue, S. J., and Bellerby, R. G. J.: Temporal variations of pCO_2 in surface seawater of the Arabian Sea in 1995, Deep Sea Research I, 45(4–5), 609–623, 1998a.

Goyet, C., Metzl, N., Millero, F., Eischeid, G., O'Sullivan, D., and Poisson, A.: Temporal variation of the sea surface CO2/carbonate properties in the Arabian Sea, Marine Chemistry, 63(1–2), 69–79, 1998b.

Goyet, C., Coatanoan, C., Eischeid, G., Amaoka, T., Okuda, K., Healy, R., and Tsunogai, S.: Spatial variation of total CO_2 and total alkalinity in the northern Indian Ocean: A novel approach for the quantification of anthropogenic CO_2 in seawater, J. Marine Res., 57, 135–163, 1999.

Haake, B., Rixen, T., and Ittekkot, V.: Variability of moonsonal upwelling signals in the deep western Arabian Sea, SCOPE/UNEP Sonderband, 76, 85–96, 1993a.

Haake, B., Ittekkot, V., Rixen, T., Ramaswamy, V., Nair, R. R., and Curry, W. B.: Seasonality and interannual variability of particle fluxes to the deep Arabian Sea, Deep Sea Research I, 40(7), 1323–1344, 1993b.

Hamm, C. E., Merkel, R., Springer, O., Jurkojc, P., Maler, C., Prechtel, K., and Smetacek, V.: Architecture and material properties of diatom shells provide effective mechanical protection, Nature, 421, 841–843, 2003.

Harrison, K. G.: Role of increased marine silica input on paleo-$p\mathrm{CO}_2$ levels, Paleoceanography, 15(3), 292–298, 2000.

Hedges, J. I., Baldock, J. A., Gelinas, Y., Lee, C., Peterson, M. L., and Wakeham, S. G.: The biochemical and elemental composition of marine plankton: A NMR perspective, Marine Chemistry, 78, 47–63, 2002.

Heinze, C.: Simulating oceanic CaCO_3 export production

in the greenhouse, Geophys. Res. Lett., 31, L16308, doi:10.1029/2004GL020613, 2004.
Heinze, C., Maier-Reimer, E., and Winn, K.: Glacial pCO_2 Reduction by the World Ocean: Experiments with the Hamburg Carbon Cycle Model, Paleoceanography, 6(4), 395–430, 1991.
Honjo, S., Dymond, J., Prell, W., and Ittekkot, V.: Monsoon-controlled export fluxes to the interior of the Arabian Sea, Deep Sea Research II, 46(8–9), 1859–1902, 1999.
Hupe, A. and Karstensen, J.: Redfield stoichiometry in Arabian Sea subsurface waters, Global Biogeochem. Cycles, 14(1), 357–372, 2000.
Hutchins, D. A. and Bruland, K. W.: Iron-limited diatom growth and Si:N uptake ratios in a costal upwelling regime, Nature, 393, 561–564, 1998.
Karl, D., Letelier, R., Tupas, L., Dore, J., Christian, J., and Hebel, D.: The role of nitrogen fixation in biogeochemical cycling in the suptropical North Pacific Ocean, Nature, 388, 533–538, 1997.
Karl, D. M., Christian, J. R., Dore, J. E., Hebel, D. V., Letelier, R. M., Tupas, L. M., and Winn, C. D.: Seasonal and interannual variability in primary production and particle flux at Station ALOHA, Deep Sea Research II, 43(2–3), 539–568, 1996.
Klausmeier, C. A., Lichtman, E., Daufresne, T., and Levin, S., A.: Optimal nitrogen-to-phosphorus stoichiometry of phytoplankton., Nature, 429, 171–174, 2004.
Körtzinger, A., Duinker, J. C., and Mintrop, L.: Strong CO_2emissions from the Arabian Sea during south-west monsoon, Geophys. Res. Lett., 24(14), 1763–1766, 1997.
Lalli, C. and Parsons, T. R.: Biological Oceanography, an introduction, 301 p., Pergamon Press Ltd, Oxford, 1993.
Lee, C. and Cronin, C.: The vertical flux of particulate organic nitrogen in the sea: decomposition of amino acids in the Peru upwelling area and the equatorial Atlantic, J. Marine Res., 40(1), 227–251, 1982.
Lee, C., Wakeham, S. G., and Hedges, I. J.: Composition and flux of particulate amino acids and chloropigments in equatorial Pacific seawater and sediments, Deep Sea Research Part I: Oceanographic Research Papers, 47(8), 1535–1568, 2000.
Lee, C., Murray, D. W., Barber, R. T., Buesseler, K. O., Dymond, J., Hedges, J. I., Honjo, S., Manganini, S. J., and Marra, J.: Particulate organic carbon fluxes: compilation of results from the 1995 US JGOFS Arabian Sea Process Study, Deep Sea Research II, 45(10–11), 2489–2501, 1998.
Liss, P. S. and Merlivat, L.: Air-sea gas exchange rates: Introduction and synthesis, in: The Role of Air-Sea Exchange in Geochemical Cycling, edited by: Buat-Mernard, P., p. 113–129, Reidel, Boston, 1986.
Maier-Reimer, E.: Dynamic vs. apparent Redfield ratio in the oceans: A case for 3D-models, J. Marine Syst., 9, 113–120, 1996.
Maier-Reimer, E., Mikolajewicz, U., and Winguth, A.: Future ocean uptake of CO_2: interaction between ocean circulation and biology, Climate Dynamics, 12, 711–721, 1996.
Matsumoto, K. and Sarmiento, J. L.: Silicic acid leakage from the Southern Ocean: A possible explanation for glacial atmospheric $p\mathrm{CO}_2$, Global Biogeochem. Cycles, 16(3), 5-1–5-23, 2002.
Measures, C. I. and Vink, S.: Seasonal variations in the distribution of Fe and Al in the surface waters of the Arabian Sea, Deep Sea Research Part II: Topical Studies in Oceanography, 46(8-9), 1597–1622, 1999.
Millero, F. J., Degler, E. A., O'Sullivan, D. W., Goyet, C., and Eischeid, G.: The carbon dioxide system in the Arabian Sea, Deep Sea Research Part II: Topical Studies in Oceanography, 45(10–11), 2225–2252, 1998.
Milliman, J. D. and Droxler, A. W.: Neritic and pelagic carbonate sedimentation in the marine environment: ignorant is not bliss, Geologische Rundschau, 85, 496–504, 1996.
Morrison, J. M., Codispoti, L. A., Gaurin, S., Jones, B., Manghanani, V., and Zheng, Z.: Seasonal variation of hydrographic and nutrient fields during the US JGOFS Arabian Sea Process Study, Deep Sea Research II, 45(10–11), 2053–2101, 1998.
Nightingale, P. D., Malin, G., Law, C. S., Watson, A. J., Liss, P. S., Liddicoat, M. I., Boutin, J., and Upstill-Goddard, R. C.: In situ evaluation of air-sea gas exchange parameterizations using novel conservative and volatile tracers, Global Biogeochem. Cycles, 14, 373–387, 2000.
Passow, U., Alldredge, A. L., and Logan, B. E.: The role of particulate carbohydrate exudates in the flocculation of diatom blooms, Deep Sea Research I, 41(2), 335–357, 1994.
Passow, U., Shipe, R. F., Murray, A., Pak, D. K., Brzezinski, M. A., and Alldredge, A. L.: The origin of transparent exopolymer particles (TEP) and their role in the sedimentation of particulate matter, Continental Shelf Research, 21(4), 327–346, 2001.
Ramage, C. S.: Monsoon Meteorology, Academic Press, New York, London, 1971.
Ramage, C. S.: Monsoon Climates, in: The Encyclopedia of Climatology, edited by: Oliver, J. E. and Fairbridge, R. W., Van Nostrand Reinhold Company, New York, 1987.
Redfield, A. C., Ketchum, B. H., and Richards, F. A.: The Influence of organisms on the composition of sea-water, in: The sea, edited by: Hitt, M., N., pp. 26–77, Wiley & Sons, New York, 1963.
Ridgwell, A. J., Watson, A. J., and Archer, D.: Modeling the response of the oceanic Si inventory to perturbation, and consequences for atmospheric CO_2, Global Biogeochem. Cycles, 16(4), 19-1–19-15, 2002.
Rixen, T., Haake, B., and Ittekkot, V.: Sedimentation in the western Arabian Sea: the role of coastal and open-ocean upwelling, Deep Sea Research II, 47, 2155–2178, 2000.
Rixen, T., Guptha, M. V. S., and Ittekkot, V.: Sedimentation, in: Report of the Indian Ocean Synthesis Group on the Arabian Sea Process Study, edited by: Watts, L., Burkill, P. H., and Smith, S., pp. 65–73, JGOFS International Project Office, Bergen, 2002.
Rixen, T., Guptha, M. V. S., and Ittekkot, V.: Deep ocean fluxes and their link to surface ocean processes and the biological pump, Progress in Oceanography, 65, 240–259, 2005.
Rixen, T., Haake, B., Ittekkot, V., Guptha, M. V. S., Nair, R. R., and Schlüssel, P.: Coupling between SW monsoon-related surface and deep ocean processes as discerned from continous particle flux meausurements and correlated satellite data, J. Geophys. Res., 101(C12), 28 569–28 582, 1996.
Sabine, C. L., Wanninkhof, R., Key, R. M., Goyet, C., and Millero, F. J.: Seasonal CO_2 fluxes in the tropical and subtropical Indian Ocean, Marine Chemistry, 72(1), 33–53, 2000.
Sarmiento, J. L., Dunne, J., Gnanadesikan, A., Key, R. M., Matsumoto, K., and Slater, R.: A new estimate of the CaCO3 to organic carbon export ratio, Global Biogeochem. Cycles, 16(4), 54-1–54-12, 2002.
Schiebel, R.: Planktic foraminiferal sedimentation and the marine calcite budget, Global Biogeochem. Cycles, 16(4), 13-1–13-21,

2002.

Schiebel, R., Zeltner, A., Treppke, U. F., Waniek, J., Bollmann, J., Rixen, T., and Hemleben, C.: Distribution of diatoms, coccolithophores and planktic foraminiferes along a trophic gradient during the SW monsoon in the Arabian Sea, Marine Micropaleontology, 51, 345–371, 2004.

Smith, S., Roman, M., Prusova, I., Wishner, K., Gowing, M., Codispoti, L. A., Barber, R., Marra, J., and Flagg, C.: Seasonal response of zooplankton to monsoonal reversals in the Arabian Sea, Deep Sea Research Part II: Topical Studies in Oceanography, 45(10–11), 2369–2403, 1998.

Smith, S. L.: Understanding the Arabian Sea: Reflections on the 1994–1996 Arabian Sea Expedition, Deep Sea Research Part II: Topical Studies in Oceanography, 48(6–7), 1385–1402, 2001.

Tegen, I. and Fung, I.: Modeling of mineral dust in the atmosphere, J. Geophys. Res., 99(D11), 22 897–22 914, 1994.

Tegen, I. and Fung, I.: Contribution to the atmospheric mineral aerosol load from land surface modification, J. Geophys. Res., 100(D9), 18 707–18 726, 1995.

Tyrrell, T.: The relative influences of nitrogen and phosphorus on oceanic primary production, Nature, 400, 525–531, 1999.

Volk, T. and Hoffert, M. I.: The carbon cycle and atmospheric CO_2, natural variation archean to present, edited by: Sundquits, E. T. and Broecker, W. S., p. 99–110, AGU, Washington, 1985.

Wakeham, S. G., Lee, C., Hedges, J. I., Hernes, P. J., and Peterson, M. L.: Molecular indicators of diagenetic status in marine organic matter, Geochimica et Cosmochimica Acta, 61(24), 5363–5369, 1997.

Wanninkhof, R.: Relationship between gas exchange and wind speed over the ocean, J. Geophys. Res., 97, 7373–7381, 1992.

Wanninkhof, R. and McGillis, W. M.: A cubic relationship between gas transfer and wind speed, Geophys. Res. Lett., 26, 1889–1983, 1999.

Weller, R. A., Baumgartner, M. F., Josey, S. A., Fischer, A. S., and Kindle, J. C.: Atmospheric forcing in the Arabian Sea during 1994–1995: observations and comparisons with climatology and models, Deep Sea Research Part II: Topical Studies in Oceanography, 45(10–11), 1961–1999, 1998.

Weller, R. A., Fischer, A. S., Rudnick, D. L., Eriksen, C. C., Dickey, T. D., Marra, J., Fox, C., and Leben, R.: Moored observations of upper-ocean response to the monsoons in the Arabian Sea during 1994–1995, Deep Sea Research Part II: Topical Studies in Oceanography, 49(12), 2195–2230, 2002.

Zeebe, R. E. and Wolf-Gladrow, D.: CO_2 In Seawater: Equilibrium, Kinetics, Isotopes, 346 p., Elsevier Science B. V., Amsterdam, 2001.

Zeltner, A.: Monsoonal influenced changes of coccolithophore communities in the northern Indian Ocean – alteration during sedimentation and record in surface sediments, in: Tübinger Mikropaläontologische Mitteilungen, pp. 103, Institut und Museum für Geologie und Paläontologie der Universität Tübingen, Tübingen, 2000.